Bioelectromagnetics 31:391–405 (2010)

Analyzing Digital Vector Waveforms of 0–3000 Hz Magnetic Fields for Health Studies

Joseph D. Bowman,* Christian K. Miller, Edward F. Krieg, and Ruiguang Song

National Institute for Occupational Safety and Health, Cincinnati, Ohio

To improve the assessment of magnetic field exposures for occupational health studies, the Multiwave® System III (MW3) was developed to capture personal exposures to the three-dimensional magnetic field vector $\mathbf{B}(t)$ in the 0–3000 Hz band. To process hundreds of full-shift MW3 measurements from epidemiologic studies, new computer programs were developed to calculate the magnetic field's physical properties and its interaction with biological systems through various mechanisms (magnetic induction, radical pair interactions, ion resonance, etc.). For automated calculations in the frequency domain, the software uses new algorithms that remove artifacts in the magnetic field's Fourier transform due to electronic noise and the person's motion through perturbations in the geomagnetic field from steel objects. These algorithms correctly removed the Fourier transform artifacts in 92% of samples and have improved the accuracy of frequency-dependent metrics by as much as 3300%. The output of the *MwBatch* software is a matrix of 41 exposure metrics calculated for each 2/15 s sample combined with 8 summary metrics for the person's full-period exposure, giving 294 summary-exposure metrics for each person monitored. In addition, the *MwVisualizer* software graphically explores the magnetic field's vector trace, its component waveforms, and the metrics over time. The output was validated against spreadsheet calculations with pilot data. This software successfully analyzed full-shift MW3 monitoring with 507 electric utility workers, comprising over 1 million vector waveforms. The software's output can be used to test hypotheses about magnetic field biology and disease with biophysical models and also assess compliance with exposure limits. Bioelectromagnetics 31:391–405, 2010.

Key words: ELF magnetic fields; exposure assessment; computer programs

INTRODUCTION

A widely recognized deficiency in extremely low-frequency (ELF) epidemiologic studies has been the exposure assessments [Kheifets et al., 2009]. Virtually all studies that measured magnetic field exposures have used the root-mean-squared (RMS) magnitude of the ELF vector (usually called the ''resultant''). However, magnetic induction and other biophysical mechanisms proposed to explain the epidemiologic associations depend on additional magnetic field properties such as the frequency spectrum, polarization, spatial orientation to the target organ, and static magnetic fields from the earth and DC electricity (WHO, 2007). By assessing exposure only with the resultant, epidemiologic studies misclassify magnetic field exposures and thereby bias their risk estimates toward the null, which reduces their power to detect associations [Carroll et al., 2006].

Only measurements of the time-dependent magnetic field vector $\mathbf{B}(t)$ (including the static magnetic field vector $\mathbf{B}_0$) are sufficient to accurately assess exposures with all proposed biophysical mechanisms:

The findings and conclusions in this paper have not been formally disseminated by the National Institute for Occupational Safety and Health and should not be construed to represent any agency determination or policy.

C.K. Miller's present address is Department of Computer Sciences, University of Texas, Austin, TX.

R. Song's present address is National Center for HIV/AIDS, Viral Hepatitis, STD, and TB Prevention, Centers for Disease Control and Prevention, Atlanta, GA.

*Correspondence to: J.D. Bowman, National Institute for Occupational Safety and Health, 4676 Columbia Parkway, Cincinnati, OH 45226. E-mail: jbowman@cdc.gov

Received for review 30 March 2009; Accepted 11 December 2009

DOI 10.1002/bem.20570
Published online 8 March 2010 in Wiley InterScience (www.interscience.wiley.com).

magnetic induction, radical pairs, ion resonance, and magnetosomes [WHO, 2007]. The ''gold standard'' for ELF exposure assessments is therefore vector waveform capture instruments such as the Multiwave® Systems II and III (Electric Research and Management (ERM), Pittsburgh, PA) and Narda EFA-300 (Narda Safety Test Solutions GmbH, Pfullingen, Germany).

To measure worker exposures to the magnetic field vector for occupational health studies, the National Institute for Occupational Safety and Health (NIOSH) collaborated with ERM to develop a personal vector waveform capture monitor, the Multiwave® System III (MW3). This instrument automatically records digital waveforms from a three-axis fluxgate magnetometer probe (0–3000 Hz) every 10 s for nearly a full shift. By feeding signals from the three probes through a fast multiplexer into a synchronized analog/digital converter, the MW3 captures the magnetic flux density vector $\mathbf{B}(t)$ at 7680 Hz for 2/15 s.

To analyze MW3's measurements from field studies, new software was developed to automatically process large batches of waveform data and explore the results graphically. The output is a wide array of magnetic field metrics (Table 1), including physical characteristics (e.g., the RMS vector magnitude of the ELF magnetic field, its frequency spectrum, and polarization) and quantities potentially important to human health (e.g., currents induced in the brain and the cyclotron resonance frequency for Ca^{2+}).

Compared with earlier software for the Multiwave System [ERM, 1997], these new programs calculate many more exposure metrics and solve scientific and technical challenges created by the MW3. The greatest scientific challenge was selecting the exposure metrics most useful in health studies from the multitude derivable from vector waveforms. The greatest technical challenge was calculating accurate fast Fourier transforms (FFT) from measurements of personal exposure to static and ultra-low-frequency (ULF) magnetic fields that affect radical pair production and other biomechanisms [Hore, 2005; Binhi, 2008]. Since a person wearing a MW3 probe often moves through perturbations in the earth's field by steel objects, magnetic field waveforms usually have aperiodic baselines that produce artifacts in their FFT (Fig. 1). Furthermore, the motion artifacts were not easily

TABLE 1. Some Exposure and Summary Metrics Calculated From Multiwave System III Data

Metric	Abbreviation	Units
Exposure metrics		
RMS vector magnitude of ELF field[a]	ELF	μT or mG
RMS magnitude of ULF (gradient) field[a]	ULF	μT or mG
RMS magnitude of ELF + ULF fields	ELF + ULF	μT or mG
Static magnetic field magnitude	B_0	μT or mG
ELF magnitude parallel and perpendicular to B_0	*B*_para, *B*_perp	μT or mG
RMS of d*B*/d*t* magnitude (with the ULF field)	d*B*/d*t*	μT/s or mG/s
Total harmonic distortion[a]	THD	Percent
Fundamental, 2nd, and 3rd freq. in spectrum[a]	FundFreq, 2ndFreq, 3rdFreq	Hz
Three largest RMS harmonic magnitudes[a]	FundMag, etc.	μT or mG
Axial ratio (minor:major axes) of fundamental, 2nd, and 3rd frequencies (polarization index)[a]	FundAxisRatio, etc.	No unit
Ratio of minimum to maximum values of $\lvert B_{\mathrm{ELF}}(t)\rvert$ (multifrequency polarization index)	Min:Max	No unit
RMS fullband magnitude (static + gradient + ELF fields)	FullbandMag	μT or mG
Maximum induced current density (*J*) in the brain	Max*J*	μA/m^2
Median *J* in the brain and heart	*J*Brain, *J*Heart	μA/m^2
Maximum induced electric field (*E*) in the brain	Max*E*	μV/m
Median *E* in the brain and heart	Ind*E*Brain, Ind*E*Heart	μV/m
Cyclotron resonance (CR) freq. for Ca^{2+}, Mg^{2+}, Zn^{2+}, Li^{+}, and H^{+}	CRFreqCa2+, etc.	Hz
Ion parametric resonance metric for Ca^{2+}, Mg^{2+}, and Zn^{2+}	IPRCa2+, etc.	No unit
3-state ion resonance metric for Ca^{2+}, Mg^{2+}, and Zn^{2+}	3StIPRCa2+, etc.	No unit
Summary metrics		
Time-weighted average (arithmetic mean)	TWA	Same as metric
Geometric mean over time	GM	Same as metric
Minimum and maximum over time	Min, Max	Same as metric
Percent time exposed (above a threshold or within a window for selected exposure metrics)	PTE	%
Rate of change metric	RCM	Same as metric
Standardized and fractional rate of change metrics	SRCM, FRCM	No unit

[a]Frequency-dependent metrics.

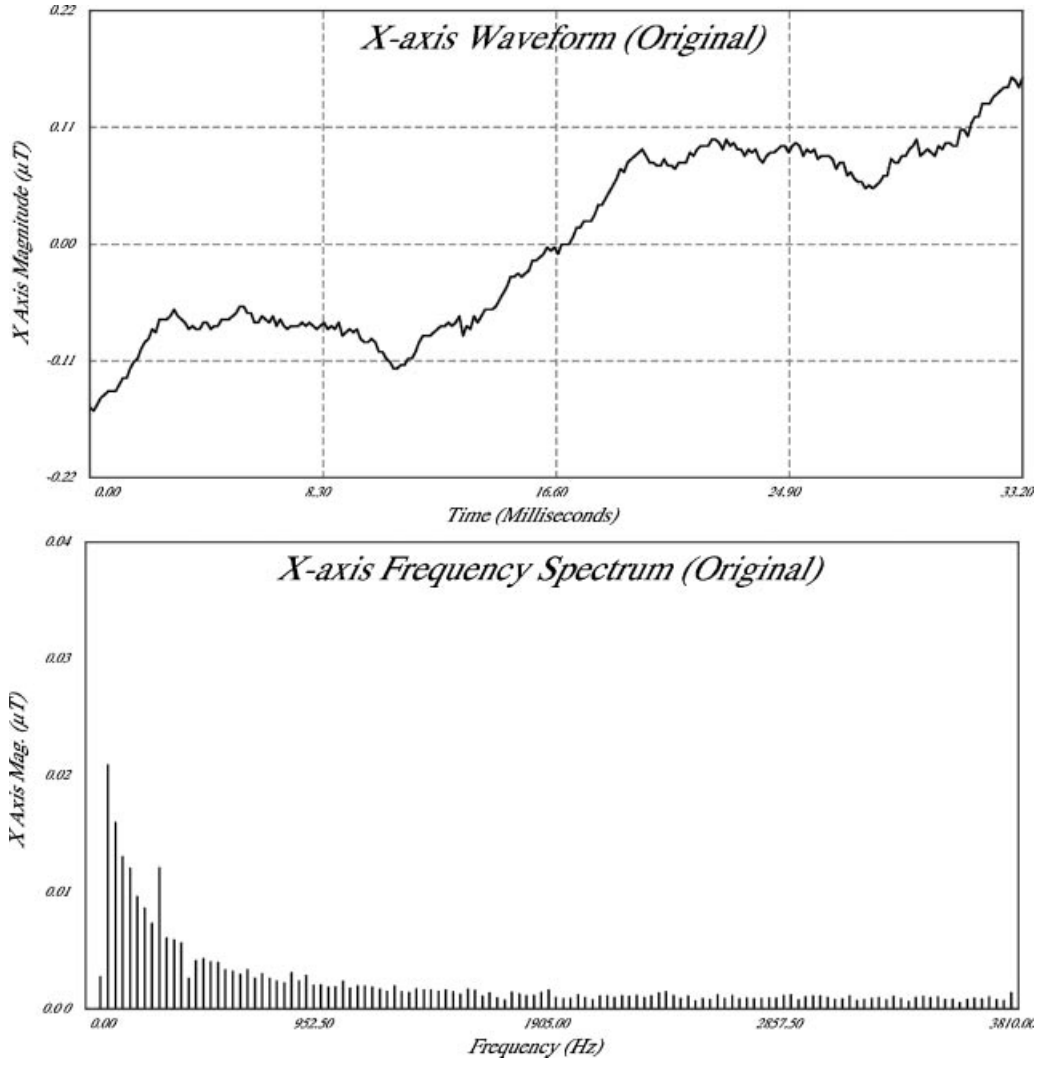

Fig. 1. Raw waveform recorded by a Multiwave System III and its fast Fourier transform (FFT), demonstrating the FFT artifacts resulting from the waveform's moving baseline. (The waveform's static component is removed and its duration reduced by a factor of $\frac{1}{4}$ by the application of a rectangular window.)

distinguishable from the MW3's electronic noise, which also needed to be removed.

This article describes the motion correction and noise removal techniques developed to analyze MW3 waveforms, plus the program architecture created to perform calculations of multiple exposure metrics and graph the large quantities of waveform data collected in health research studies.

METHODS

Instrument

The MW3's fluxgate magnetometer probe (Bartington Instruments, Oxon, UK) responds to both static (DC) and ELF magnetic fields [Campbell, 1997]. If the signal from any of the three vector components is out of range, the MW3's built-in amplifier switches from high gain ($\times 10$) to low gain for the entire waveform, giving a dynamic range of 0.002–1000 μT peak for each component. The analog signals from the three fluxgate probes are then fed into a built-in 45 kHz multiplexer and digitized at a 7680 Hz rate over a time window $T = 2/15$ s, giving synchronized 1024-point waveforms for each vector component.

This sampling configuration gives the waveform's FFT with a base frequency Δf of 7.5 Hz. This arrangement can analyze both 60 Hz fields from North American AC electricity and 75 Hz fields from older computer monitors with cathode ray tubes without

windowing the waveforms. Since 7.5 Hz is also greater than the time-varying components of the geomagnetic field [Campbell, 1997], this is an excellent configuration for monitoring magnetic fields in workplaces and residences.

In a regular run, the MW3 will capture a vector waveform sample every 10 s and record the data on a 16-MB flash card. It can take these readings for up to $7\frac{1}{2}$ h, yielding a maximum of 2716 samples. After monitoring is complete, the flash card is transferred to a PC so that the data can be downloaded for analysis by the MW3's software.

Motion Correction

A person moving in the modern electromagnetic environment often encounters waveforms that are not periodic (Fig. 1). Aperiodic waveforms may be due to the person's motion relative to the EMF source, rapidly changing currents in AC sources, or the person's motion through gradients in the earth's magnetic field perturbed by steel objects.

The FFT algorithm assumes that a discrete waveform $\{B(t) \ | 0 \leq t \leq T\}$ is replicated out to $t = \pm\infty$, which turns an aperiodic $B(t)$ into an artificial sawtooth-like pattern. Consequently, many of the resulting Fourier coefficients are dominated by these sawtooth artifacts, which decrease with frequency from a peak at its base frequency (Fig. 1).

These FFT artifacts must be removed if magnetic field characteristics are to be calculated accurately in the frequency domain. Therefore, we developed an algorithm for removing the FFT artifacts, which result from a stationary ELF signal superimposed on a moving baseline [Supplementary Online Material (SOM), 2010a]. The effects of this motion correction algorithm on the waveform and the FFT are shown in Figure 2.

However, this algorithm will not remove FFT artifacts caused by factors other than a moving baseline (e.g., non-periodic ELF signals in Fig. 3). In order to assure accurate calculations with the FFTs, a numerical test for residual FFT artifacts was developed for the Multiwave software. First, we created several indices that quantified the waveform's periodicity and the characteristic artifact pattern in the FFT (Fig. 1). These indices included the difference between the waveform's start and stop points (a periodicity test), the "lagged difference" between all points in two halves of the waveform, distortion from non-harmonics, and a downward trend in the low-frequency end of the FFT [SOM, 2010b]. However, no single index could reliably detect motion artifacts that were obvious in visual inspections of corrected waveforms and their FFTs.

In order to derive a motion test with multiple indices, we therefore performed a discriminant analysis of 200 measured waveforms after the application of the motion correction algorithm. Two samples of 100 waveforms whose magnitudes were well above noise ($>0.05\ \mu$T) were randomly selected from MW3 measurements from a study of electric utility workers at Southern California Edison [Bowman et al., 2010]. After applying the motion correction algorithm, each corrected FFT was visually checked for the absence of the characteristic artifact pattern (Fig. 1) and the corrected waveform was checked for periodicity, based on the match of its start and stop points, constancy of peak amplitudes, and regularity of the zero crossing points. Based on this visual inspection, the corrected waveform was placed into a "success" or "failure" group. In addition, the candidate motion indices were calculated for all waveforms. These indices were formulated so that they are zero in the absence of artifacts and become larger as the artifacts grow more prominent.

Stepwise discriminant analysis was then performed using the DISCRIM procedure with the STEPDISC option in SAS® [SAS, 2003]. Candidate motion indices were entered stepwise into quadratic discriminant functions for success or failure [SOM, 2010b]. The P-value for a term to enter or leave the discriminant model was $P = 0.15$. The most consistent results were obtained when the samples were combined, yielding success and failure discriminant functions [SOM, 2010b]. When the success function has a larger value than the failure function, the motion artifacts in a waveform's FFT are considered minimal so that frequency domain calculations can be performed.

Noise Removal

The MW3 was designed with RMS electronic noise less than $0.002\ \mu$T, which is adequate for measuring the RMS ELF vector magnitudes encountered in the environment. However, our software also calculates dB/dt as a first step in calculating induced body currents [SOM, 2010e], and this requires lower electronic noise. Therefore, we developed two noise removal algorithms: a digital gain filter when the motion correction succeeded in removing the FFT artifacts, and spline smoothing when motion correction failed.

If motion correction succeeds, the frequency spectrum has only signal and noise frequencies (Fig. 2), so a digital gain filter can be used. Frequency-dependent cutoffs for the gain filters were determined by an analysis of the MW3s' calibration data [SOM, 2010c].

The resulting cutoff curves for high and low gain had floors set above the majority of the noise FFT magnitudes (Fig. 4). Where the calibration data had noise peaks above the floor, the cutoff curves were set

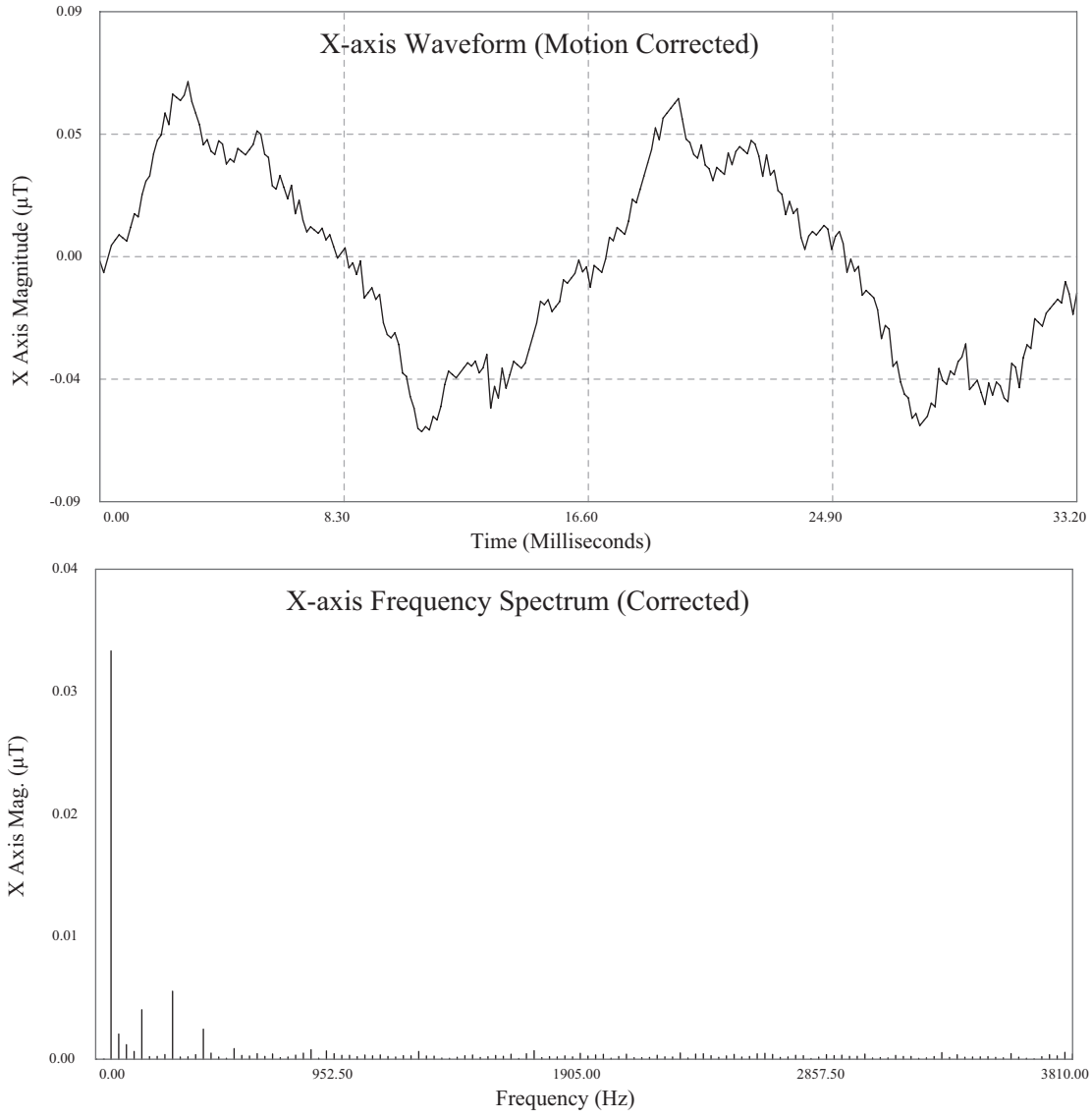

Fig. 2. The waveform in Figure 1 after motion correction. The waveform is now periodic, and motion artifacts in the FFT are eliminated.

equal to those peaks. The eight MW3 instruments had cutoff floors ranging from 0.0006 to 0.0032 μT at high gain and 0.0033 to 0.0055 μT at low gain. Their filters had between 11 and 32 peaks above the cutoff floors with maximums from 0.0019 to 0.0097 μT at high gain. At low gain, the filter had between 5 and 50 peaks with maximums from 0.006 to 0.033 μT.

In the software, the digital filter subroutine applies the noise cutoffs to every frequency in a sample's FFT, setting to zero all magnitudes whose measurement is below their cutoff and leaving all other values unchanged. This produces the filtered frequency spectrum, which is run through an inverse FFT to obtain the final smoothed waveform (Fig. 5).

When the motion correction fails, the motion artifacts defeat a digital filter, so the noise is removed by a smoothing cubic spline [Reinsch, 1967]. A cubic spline function consists of piece-wise third-order polynomials for each interval $[B(t_i), B(t_{i+1})]$ in the digital waveform. The cubic spline algorithm determines the polynomial coefficients by requiring that the second derivatives of adjoining pieces match at their intersections [Press et al., 1988]. In spline smoothing, this continuity requirement is maintained for the piecewise functions, but the spline function $B_{sp}(t)$ no longer runs through all the data points $B(t_i)$. Instead, the polynomial coefficients are determined by minimizing the functional:

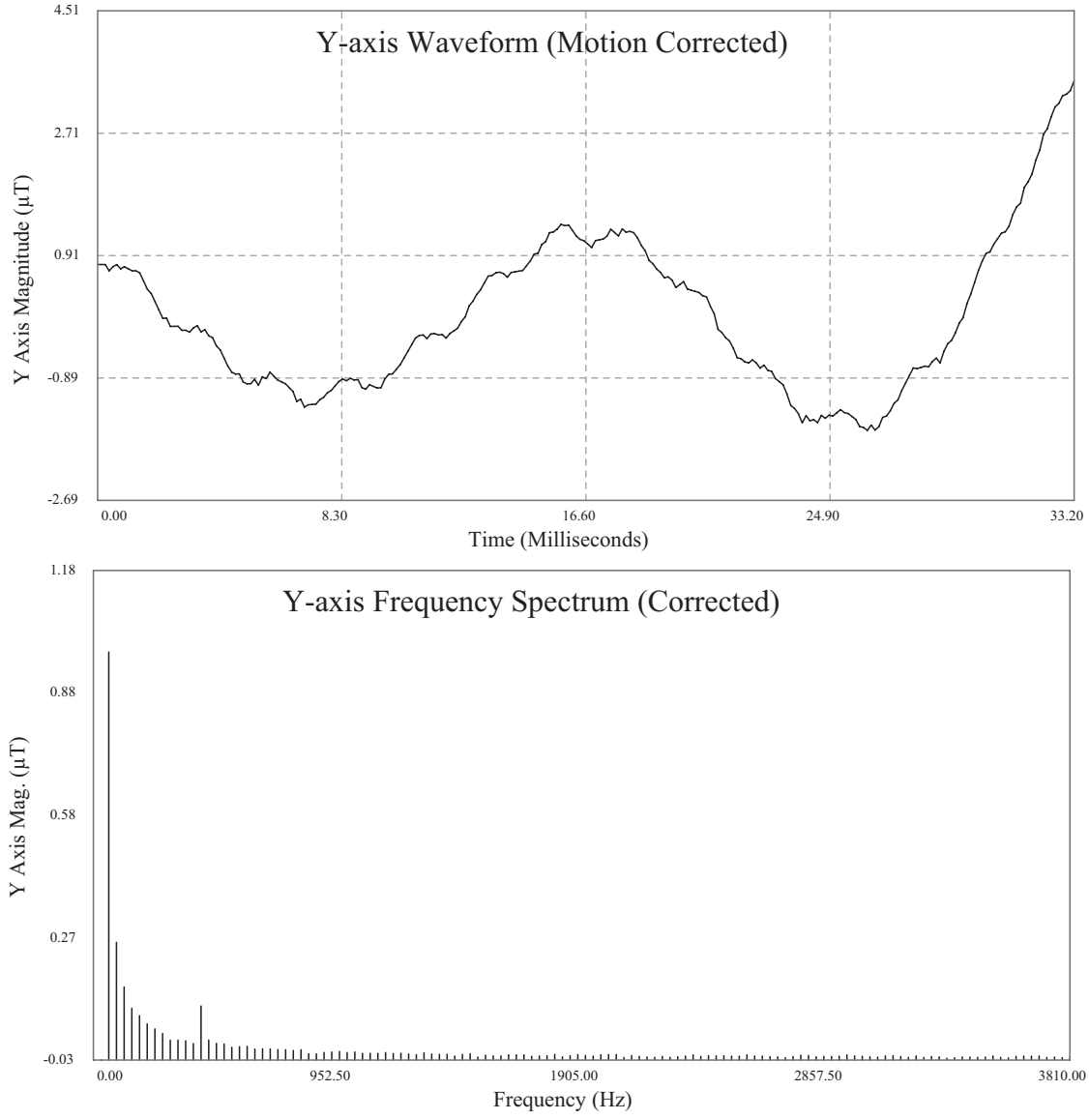

Fig. 3. An aperiodic waveform (different from Figs. 1 and 2) where the motion correction algorithm was unsuccessful in removing the FFT artifacts.

$$\sum_i \left(B_{\mathrm{sp}}(t_i) - B(t_i)\right)^2 + \lambda \int B''_{\mathrm{sp}}(t)^2 \, \mathrm{d}t \qquad (1)$$

The optimal value for the smoothing parameter λ equals s_t^2/N, where s_t is the standard deviation (SD) from the noise in the time domain and N is the number of data points in a waveform [Reinsch, 1967].

The noise SDs s_t for the MW3 instruments were determined from the calibration waveforms by removing the FFT components of their signal frequencies (0, 60, 120, 180, and 300 Hz), and taking the SD of the remainders. Like the noise spectrum, the noise SD varied with the gain and the MW3 serial number. With these values for λ as input, the coefficients for the cubic spline are calculated by the Reinsch algorithm with the assistance of a C++ subroutine for cubic spline interpolation [Press et al., 1988]. The time derivative $\mathrm{d}B(t)/\mathrm{d}t$ is calculated by taking the derivative of the spline's cubic polynomials.

A drawback of spline smoothing is that it tends to flatten sinusoidal peaks, producing a negative bias in RMS[$|\mathrm{d}\mathbf{B}/\mathrm{d}t|$]. We therefore developed an algorithm for correcting this bias from an analysis of sine waves with random noise [SOM, 2010d].

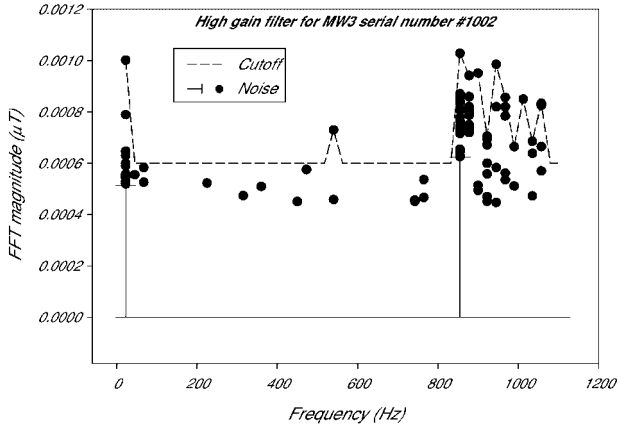

Fig. 4. Box-and-whisker plots of noise FFT magnitudes (192 points per frequency) extracted from calibration data for one Multiwave System III, plus the cutoff set for its digital filter. (Every third noise harmonic from 22.5 to 1200 Hz is plotted. Higher frequencies up to 3840 Hz are not shown.)

Exposure and Summary Metrics

After smoothing a vector waveform, the Multiwave's software calculates the magnetic field *exposure metrics* for each vector waveform (Table 1).

Exposure metrics at the top of Table 1 are physical characteristics of the magnetic field, many of which have been used previously in EMF exposure assessments [Bowman, 1998]. An innovative physical metric in this software is a polarization metric for multifrequency fields called "Min:Max," the ratio of the minimum to the maximum ELF magnitudes $|\mathbf{B}_{\mathrm{ELF}}(t)|$. A more familiar polarization index is the axial ratio, the minor axis divided by major axis. However, that index must be calculated for each frequency in the magnetic field's spectrum (Fig. 8). Min:Max has the same interpretation as the axial ratio for single-frequency fields ($0 \Rightarrow$ linear polarization; $1 \Rightarrow$ circular polarization), but uses only one number to summarize the deviation of a multifrequency field from linear polarization.

The static magnetic field $\mathbf{B}_0$ and its interaction with $\mathbf{B}_{\mathrm{ULF+ELF}}(t)$ required another set of exposure metrics, like the static field magnitude B_0, FullbandMag = RMS[$|\mathbf{B}_0 + \mathbf{B}_{\mathrm{ULF+ELF}}(t)|$], and B_para = RMS[$\mathbf{B}_0 \bullet \mathbf{B}_{\mathrm{ELF}}(t)$]. These metrics are useful indicators of magnetic field interactions with biological magnetic moments, like radical pairs [Hore, 2005] and magnetite [Polk, 1994].

The electric fields induced in the brain and heart are estimated by combining the MW3's measurements of $\mathrm{d}\mathbf{B}(t)/\mathrm{d}t$ with finite-difference time-domain (FDTD) dosimetry [SOM, 2010e]. We used FDTD results for homogeneous, linearly polarized 1 μT, 60 Hz magnetic fields aligned with the principal axes of a high-resolution male model [Gandhi et al., 2001]. The NIOSH software performs these calculations for the FDTD voxels for the median-induced fields within the heart and brain and the maximum field in the brain. The final metrics listed in Table 1 are the RMS induced electric fields and current densities RMS[$|\mathbf{J}|$] = σ RMS[$|\mathbf{E}|$], where σ is the conductivity in the target organ.

With regard to safety guidelines, the maximum induced field within the brain Max$E$ can be compared to the basic restriction of the Institute of Electrical and Electronic Engineers [IEEE International Committee on Electromagnetic Safety, 2002], and the maximum current density Max$J$ can be compared to the basic restriction of the International Commission on Non-Ionizing Radiation Protection [ICNIRP, 1998] The algorithm in the NIOSH software [SOM, 2010e] calculates induced fields and currents accurately if the three-dimensional sensors in the MW3 probe are aligned with the principal axes of the body (which is feasible) and the magnetic field is homogeneous over the person's body (which is seldom the case).

Finally, we calculated three ion resonance metrics with a selection of ions for which biological resonances had been reported [Binhi, 2002]. The ion parametric resonance (IPR) metrics were calculated with the analytic formula derived from basic principles [Lednev, 1995]. Applying the IPR formula to an arbitrary vector waveform $\mathbf{B}(t)$ assumes that the ion's binding site has an axis of symmetry aligned with the static field vector $\mathbf{B}_0$ [Bowman et al., 2005]. The three-state ion resonance model assumes that the ion's binding site is a symmetric tetrahedron or octahedron, from which Engstrom and Bowman [2004] derived the differential equation:

$$\frac{\mathrm{d}p(t)}{\mathrm{d}t} = \left(\frac{q}{2m}\right)\mathbf{p}(t) \times \mathbf{B}(t) \qquad (2)$$

where q/m is the ion's charge-to-mass ratio and $\mathbf{p}(t)$ is the modulation of the transition electric dipole for transitions between the ion's ground and first excited vibrational states. In the software, Equation (2) is solved numerically for electric dipole's component in the direction $\hat{n}$ where the ion would dissociate from the protein. Assuming that all such ion–protein complexes in the body are aligned arbitrarily in space, the software averages RMS[$\mathbf{p}(t) \bullet \hat{\mathbf{n}}$] over all dissociation directions $\hat{n}$ to obtain the three-state IPR metrics for Ca^{2+}, Mg^{2+}, and Zn^{2+}.

Forty-two exposure metrics (plus the motion correction indices) are calculated for each vector waveform and stored in a database with their time and subject ID for later processing. For each subject, the

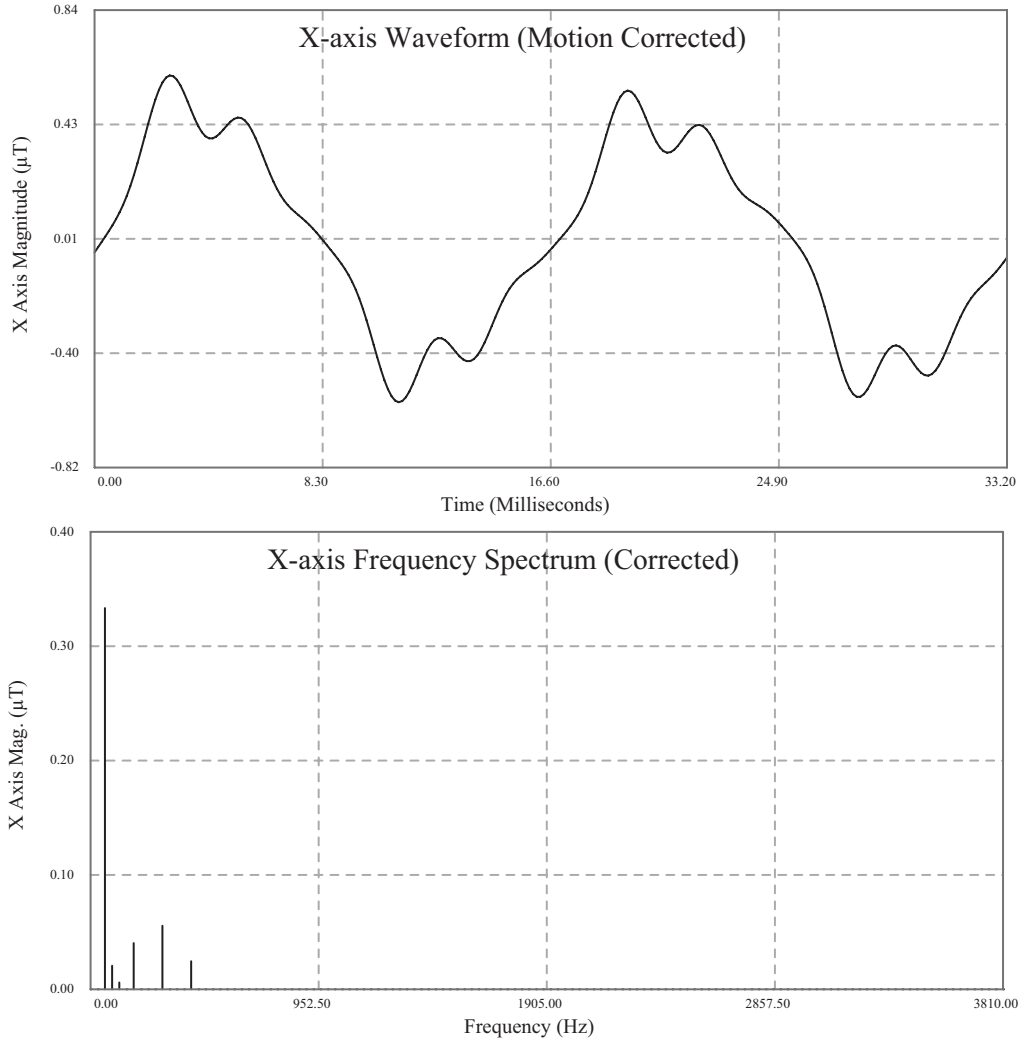

Fig. 5. The final waveform from Figure 1 with motion corrected and smoothed by the digital filter. Such a waveform is suitable for calculating all metrics in the time or frequency domains.

summary metrics in Table 1 are then calculated for all exposure metrics. The summary metrics include basic statistics such as the MIN, MAX, time-weighted average (TWA), and SD, plus metrics derived from EMF health studies. The PTE metric (''percent time exposed'' above a threshold or within a window) requires the entry of threshold values, which are currently set at 1 μT for ELF, 10 μT for ELF + ULF, and 60 ± 8 Hz for cyclotron resonance frequencies [Bowman et al., 1995]. (For other exposure metrics that are not assigned thresholds, the PTE summary metric is not calculated.) The three ''rate of change'' metrics in Table 1 had been created to study intermittent exposures in epidemiology [Burch et al., 1999; Kaune et al., 2001]. Because the rate of change metrics depend on adjacent values in a metric's time series, their calculations for frequency-dependent metrics compensate for gaps where the motion correction failed.

The software's primary output is a matrix of 347 combinations of summary and exposure metrics for each subject. Table 2 shows a selection of these *summary-exposure metrics*, which are given abbreviations such as TWA–THD, SD–Min:Max, and PTE–ELF.

Program Architecture

The MW3 suite of programs (NIOSH, Cincinnati, OH) consists of an analysis program (*Mw3Batch*), a pre-programmed Microsoft *Access*® database (*Mw3Output*), and a graphics program (*MwVisualizer*). Figure 6 outlines their connections as a flow chart.

The *Mw3Batch* analysis software processes all vector waveforms in a batch of MW3 files, including the motion correction, noise removal, and calculation of 47 exposure metrics from each waveform (Table 1). It was designed to handle large sets of data in a field study

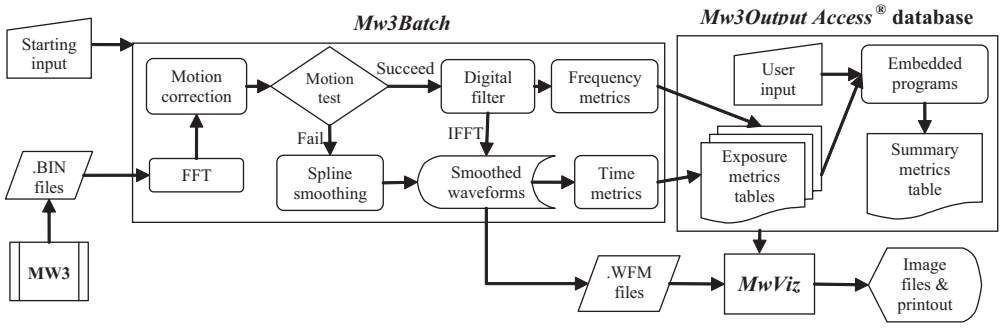

Fig. 6. Flow chart for the Multiwave suite of programs, showing the data paths from the binary files produced by the Multiwave® System III (MW3) to the summary metric outputs (Table 3) and graphic images (Figs.1–3, 5, and 7–9).

with minimal user interaction, and to store its output in the *Mw3Output* database. More details on the *Mw3Batch* software are in the Supplemental Online Material [SOM, 2010f].

All exposure metrics calculated from a batch of MW3 measurements then go to the *Mw3Ouput* database [SOM, 2010f]. This *MS Access*® file has an embedded program that calculates the summary metric and outputs the results to a new *Access* table (Table 2). Other imbedded programs provide for: (1) manual entry of job, environment, and task data for each subject; (2) summary reports on all data files, which the field staff can use to track measurements and check for instrument malfunctions; and (3) the export of selected data on each subject to an *Excel* file, which can then be merged with a report letter and given to the workers to summarize their exposures.

The *MwVisualizer* (*MwViz*) program [SOM, 2010f] was created to graph the magnetic field waveforms and their exposure metrics measured during a study. When directed to the output database for a set of subjects, *MwViz* produces plots of any selected metric over time (Fig. 7). By clicking on a time plot, the vector waveforms and their FFTs for that instant are displayed (Fig. 5), including a three-dimensional plot of the vector's trace (Fig. 8). During software development, the quick visual feedback from *MwViz* was a key tool in validating the results of *Mw3Batch* and *Mw3Output*. This feature also assisted in the development of the motion test [SOM, 2010b] and noise filters [SOM, 2010c].

Software Validation

All outputs from these programs were validated with half-shift measurements from a pilot study [McDevitt et al., 2002]. *Mw3Batch* was validated by using its option to output text files with complete waveforms and FFTs (raw and smoothed) for selected

TABLE 2. Portion of a *MwOuput* Table With a Selection of the Subjects, Summary Metrics, and Exposure Metrics Calculated From a Single Batch of MW3 Data Files

FieldName	SubjectID	Max	TWA	RCM	PTE
$\mathbf{B}_0$	21024339	139.4	42.3	7.2	NA
ELF	21024339	7.622	0.648	0.246	22.52[a]
ELF + ULF	21024339	7.762	0.591	0.417	0.00[b]
*B*_para	21024339	6.094	0.319	0.247	NA
*B*_perp	21024339	7.748	0.462	0.388	NA
d*B*/d*t*	21024339	2928.2	207.1	87.0	NA
THD	21024339	2.980	0.078	0.012	NA
FundAxisRatio	21024339	89.91	11.48	4.27	NA
FullbandMag	21024339	139.4	42.3	7.2	NA
Ind*E*Brain	21024339	51.044	2.485	1.632	NA
Ind*E*Heart	21024339	48.584	2.938	1.546	NA
Max*E*	21024339	245.71	13.985	8.176	NA
CRFreqCa2+	21024339	106.7	32.4	5.5	2.21[c]
$\mathbf{B}_0$	21024340	89.6	58.1	3.9	NA
ELF	21024340	2.316	0.215	0.096	0.12[a]

NA, not applicable → neither threshold nor window defined for this metric.
[a]ELF > 1 μT.
[b]ELF + ULF > 10 μT.
[c]52 Hz < CRFreqCa2+ < 68 Hz.

TABLE 3. Improvements in the Accuracy and the Approximate Signal-to-Noise Ratio (SNR) for Selected Exposure Metrics as a Result of the Motion Correction (MC) Algorithm and the Digital Noise Filter

	Metric value (SNR and % improvement in accuracy)		
Metric (units)	Raw waveform	Motion correction	MC and noise filter[a]
ELF (μT)	0.1337 (3.0 dB)	0.1093 (37.4 dB, +22.3%)	0.1093 (<0.1%)
d*B*/d*t* (μT/s)	2269.47 (−33.9 dB)	67.16 (−0.6 dB, +3279%)	45.86 (+46%)
FundFreq (Hz)	60.0	60.0 (0%)	60.0 (0%)
2ndFreq (Hz)	90.0	420.0 (−79%)	420.0 (0%)
FundMag (μT)	0.1029 (not defined[b])	0.1090 (54.4 dB, −6%)	0.1090 (<0.1%)
2ndMag (μT)	0.0222 (−5.9 dB)	0.0100 (>65 dB, +122%)	0.0100 (<0.1%)

Calculations are for the three-dimensional vector waveform whose *X* component is shown in Figures 1, 2, and 5.
[a]Assumed to be the signal in calculating SNRs (Eq. 4).
[b]This SNR for FundMag is undefined with this waveform because its denominator is negative. The uncorrected RMS magnitude of the fundamental is less than the ''signal'' in this measurement because the corresponding Fourier coefficient of the motion artifact happens to have a phase opposite to the signal's phase.

samples. The graphs from *MwViz* were used to identify samples with the characteristics desired for each validation. Text files for these samples were imported into spreadsheets where all calculations were replicated and compared with the values in the *MwOuput* tables. The *MwOutput* subroutines for calculating summary metrics [SOM, 2010f] were also validated by comparison with spreadsheet calculations. In these test calculations, the Min and Max summary metrics were scanned to assure that all metrics were within their mathematical limits. All discrepancies found in these quantitative and graphical validations were immediately investigated, and any software errors were corrected.

We quantified the effectiveness of the noise removal and motion correction algorithms by the improvement in the accuracy of selected metrics x for the sample waveform (Fig. 1), measured either as percent improvement in accuracy for metric x:

$$\frac{x_{\text{before}} - x_{\text{after}}}{x_{\text{after}}} \times 100\% \tag{3}$$

or its ''signal-to-noise'' ratio in dB:

$$\text{SNR}_x = 10 \log_{10} \left(\frac{x^2_{\text{signal}}}{x^2_{\text{uncorrected}} - x^2_{\text{signal}}} \right) \tag{4}$$

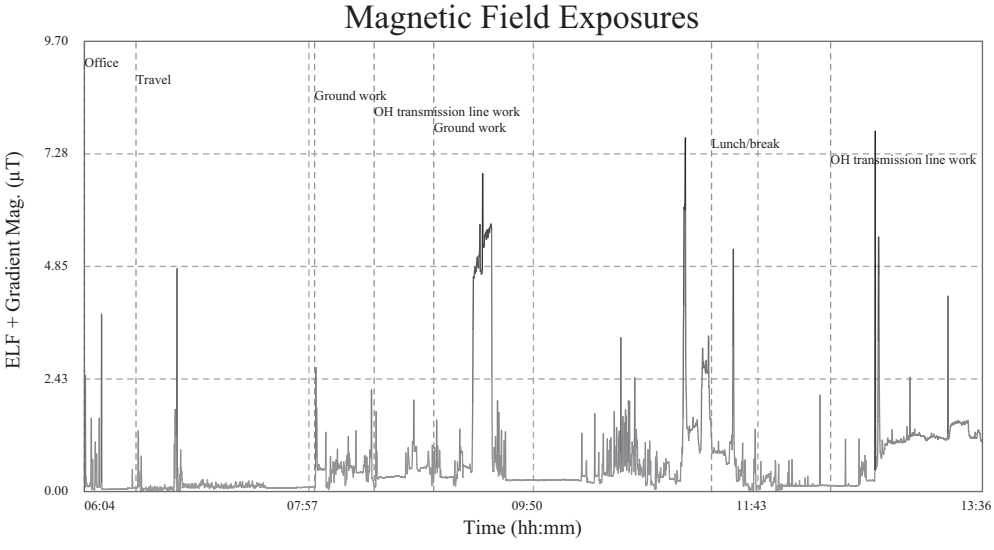

Fig. 7. MwVisualizer plot of the ELF + ULF metric versus time, showing manually entered annotations of tasks for an electric line worker.

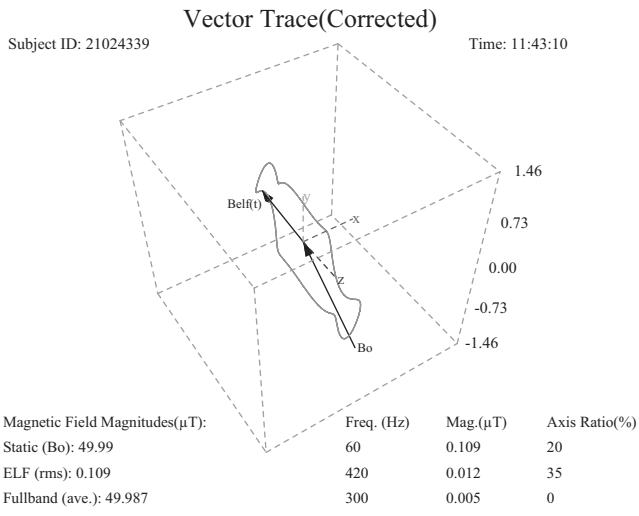

Fig. 8. MwVisualizer plot of the vector trace of the measurement whose *X*-axis waveform is shown in Figure 5, including the sample's more important physical metrics.

where the ''signal'' for x is assumed to be its value after both the motion correction and noise filtering. The ''noise'' can therefore include the motion artifacts and also the electronic noise.

RESULTS

An unprocessed MW3 waveform like Figure 1 usually gives inaccurate results for frequency-dependent metrics and the induced body currents, due to motion artifacts and electronic noise. For the selected metrics in Table 2, the signal-to-noise ratios (Eq. 2) range from 3.0 dB for the RMS vector magnitude in the ELF frequency band to a remarkable −30.6 dB for RMS[dB/dt]. Only the 60 Hz fundamental frequency in the FFT is correct in this example.

The motion correction algorithm makes dramatic improvement in the accuracy of many frequency-dependent metrics. The percent improvements in accuracy range from 6% for the fundamental RMS magnitude (FundMag) to 3300% for RMS[dB/dt]. The SNR for the ELF metric improves to 37.4 dB but is still poor (−0.6 dB) for the dB/dt metric because of the electronic noise.

The automatic motion test has also shown remarkable success. Of the 200 waveforms used to develop the test [SOM, 2010b], the discriminant classifications were in 92% agreement with the visual classification.

The algorithm's ability to correct the FFT artifacts depend on the ELF magnitude. For 580 samples from our field data [Bowman et al., 2010], those with ELF magnitudes greater than 0.4 μT had a 72.0% correction success rate, and those with lower magnitudes had a 49.4% success rate. The algorithm's failure at low magnitudes resulted from the waveform's low SNR. Noise from the MW3 tends to dominate small signals, leaving a tangled mess of a waveform which the algorithm has trouble smoothing. With low SNR waveforms, *Mw3Batch* replaced metrics such as ELF magnitude with each instrument's limits of detection, defined as three times its noise SD.

The noise SD s_t was calculated for use in the spline smoothing algorithm (Eq. 1) and averaged 0.0044 μT (range: 0.003–0.007 μT) for the eight MW3 instruments manufactured for health studies. This noise level is adequate for measuring the ELF magnitude, which is generally above 0.01 μT in workplaces. However, the higher frequency noise creates unacceptable errors in dB/dt measurements (e.g., SNR = −0.6 dB in Table 2), which are required for magnetic induction models. The high-frequency spikes (Fig. 4) are especially problematic and may be resonances from the interactions between MW3's electronic components.

In most cases, the digital filter and spline smoothing techniques successfully eliminated the electronic noise, as shown in the example waveform (Fig. 5 and Table 3). With this example, the only detectable improvement in accuracy from the noise filtering came with RMS[|d**B**/dt|] (+46%), which heavily weights the MW3's high-frequency noise (Fig. 4). Although the noise impact on other lower frequency RMS metrics in this example is less than 0.1%, we still implemented this intricate noise filter because dB/dt is the input for calculating the induced internal electric field [SOM, 2010e]. If the motion correction fails for any reason, the spline smoothing technique and its bias correction can typically salvage an acceptably clean waveform for a time-domain calculation of RMS[|d**B**/dt|].

Another common reason for motion correction failure is an aperiodic waveform (i.e., the signal changed in mid-reading like Fig. 3). To reduce the proportion of aperiodic waveforms, the software provides an option to apply a rectangular window to the time domain data that reduces the sample time T by a factor of $\frac{1}{2}$ or $\frac{1}{4}$. The waveforms in the figures have been windowed by one-quarter, which gives their FFT a base frequency $\Delta f = 30$ Hz. By reducing the MW3's 2/15 s sample duration, the waveform is less likely to include an aperiodic signal that will defeat the motion correction and create gaps in the time series of the frequency-dependent metrics. However, truncating waveforms not only discards potentially important exposure data, but in the ion resonance mechanism [Engstrom and Bowman, 2004], flattens any resonances

in those metrics. Therefore, the best strategy for epidemiologic studies is to analyze the MW3 data with both the full waveform and narrowest window.

This software enables the MW3 to be used effectively for personal monitoring in field studies. The software's first application was a study of magnetic field exposures of electric utility workers conducted at Southern California Edison in 2002–2003 [Bowman et al., 2010]. The study yielded 507 valid data sets with 2507 vector waveforms on average. This amounts to 1.27 million individual waveforms, comprising 2.4 GB of raw data.

The automated analysis and graphing architecture described here enabled the field technicians to conduct complicated analyses for a million waveforms with no training in Fourier analysis. After downloading the Multiwave's binary file and entering an ID number, start time of the monitoring and job title, the calculations required no further supervision and generated summary reports for each day's measurements that helped detect instrument malfunctions.

The *MwViz* graphics software has proved invaluable for visually exploring the vast data sets for the electric utility workers. We have identified unusual peaks in the calculated metrics, examined their waveforms, and recognized how they occurred. Figure 9 shows two unusual waveforms that were identified with *MwViz* because their abnormally high harmonic distortion produced peaks in the worker's induced body currents. This interactive graphical inspection of vector waveforms is an important tool for understanding the relationship between the EMF environment and its biophysical interactions with the human body.

DISCUSSION

The Multiwave System III vector waveform monitor combined with the *Mw3Batch* and *MwVisualizer* software is a breakthrough in assessing occupational exposures to ELF magnetic fields for health studies. Although the TWA resultant has been the chosen magnetic field metric in most influential

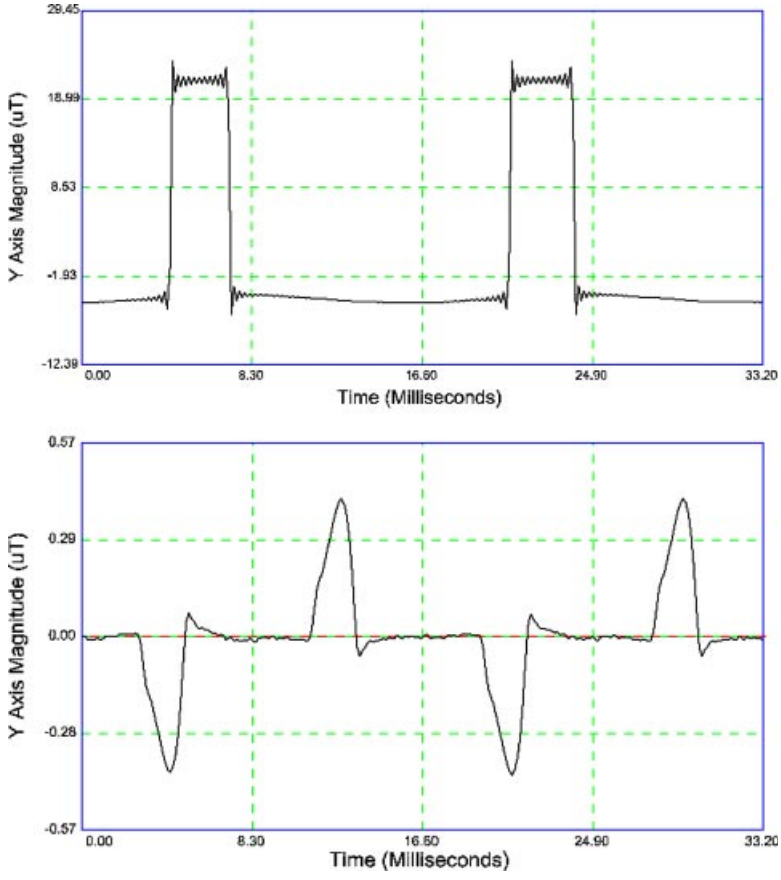

Fig. 9. Unusual waveforms identified by MwVisualizer in MW3 measurements taken on an electrician in a substation switchyard (**upper plot**) and a supervisor in an office at a steam generating station (**lower plot**).

epidemiologic studies [Kheifets et al., 2009], its faults in representing human responses to ELF magnetic fields were recognized long ago [Morgan and Nair, 1992] and will misclassify exposures in risk analyses. Depending on the correlation between the TWA resultant and the true dose metric, the ''classical measurement errors'' from the metric's misspecification could have reduced the apparent power of previous ELF studies by as much as 50% [Carroll et al., 2006]. However, the reliance on RMS gaussmeters such as the EMDEX limited explorations of alternatives to different summary metrics of the resultant [Savitz et al., 1994; Zhang et al., 1997; Villeneuve et al., 1998]. To assess exposures with more biologically relevant metrics, researchers realized that new instrumentation and better models of the relevant biophysical mechanisms would be needed [Bowman et al., 2000]. The *MwBatch* software combined with vector waveform monitors now makes the measurement of biologically based metrics feasible for ELF epidemiology.

From the earliest discussions of alternative EMF exposure metrics, researchers have debated whether epidemiologic studies should focus on a few metrics with the strongest experimental and theoretical support or just ''measure everything'' [Bowman et al., 2000]. Skeptics of the ''measure everything'' strategy have been concerned that testing all possible metrics would likely lead to spurious associations that are purely due to chance. This multiple comparisons problem is heightened by the 294 combinations of summary and exposure metrics generated by *Mw3Output*.

To minimize chance associations from the multiple comparisons, epidemiologic studies will need some sophistication. At a minimum, all 294 summary-exposure metrics need not be analyzed. The risk analysis can be limited to metrics associated with health effects in previous studies or those arising from well-defined biophysical mechanisms such as induced body currents [SOM, 2010e] or ion resonance [Engstrom and Bowman, 2004]. Multivariable statistical techniques have been used in analyzing multiple summary metrics of the ELF resultant [Zhang et al., 1997; Villeneuve et al., 1998] and other agents [Burstyn, 2004]. To test whether multiple associations with EMF summary-exposure metrics accord with other knowledge, Bayesian techniques developed for genetic epidemiology [Friedman, 2004] can be adapted to EMF. Although challenging, multiple exposure metrics derived from biological mechanisms have been used successfully to improve epidemiologic studies of ozone [Kriebel and Smith, 1990], metal-working fluids [Woskie et al., 1994], silicon carbide [Ballew et al., 1995], and asbestos [Stayner et al., 2008].

Another problem is that our software assumes the magnetic field's principle frequency is 60 Hz since it was developed for studies of North American electric utilities workers. To analyze the 50 Hz AC fields in the rest of the world or the specialized AC electricity in airliners and railroads, the motion correction algorithm, digital noise filter, and frequency-dependent metric subroutines can easily be re-programmed.

A final problem has been that vector waveform capture monitors are expensive instruments that are becoming rare with the decline of ELF epidemiologic research. ERM, the manufacturer of the Multiwave instruments, has gone out of business. The only instrument of this type still on the market, the Narda EFA-300, captures vector waveform data only from spot measurements of the ELF magnetic fields. Although our software can be modified to analyze the data collected by the Narda meter, only personal monitoring of the ELF and static magnetic field waveforms can accurately measure exposures to biologically based exposure metrics like induced body currents and ion resonance. Alternatively, our induced brain current subroutines, Max$E$ and Max$J$, could be programmed into a direct reading monitor in order to quickly measure compliance with ELF exposure limits [ICNIRP, 1998; IEEE, 2002].

CONCLUSIONS

The *MwBatch* and *MwVisualizer* suite of software is a powerful research tool for studying pressing questions in ELF exposure assessment and epidemiology [Kheifets et al., 2009]. The software was validated against spreadsheet calculations with pilot data and successfully analyzed over 500 full-shift exposure measurements on electric utility workers. By providing solutions to the many technical problems in analyzing vector waveform data, the *Mw3Batch* and *MwVisualizer* software make the measurement of worker exposures to biologically based metrics of ELF and static magnetic fields feasible for epidemiologic studies.

ACKNOWLEDGMENTS

We gratefully acknowledge the expert assistance from Electric Research and Management, especially William Gish for creating the motion correction algorithm, and George Batrus and Terrance Whittemore for developing the software. Huiqin Yan and Huazhou Liu from the Department of Electrical and Computer Engineering and Computer Science at the University of Cincinnati wrote the *MwBatch* software. Steven Jeffers from NIOSH programmed its Windows interface.

REFERENCES

Ballew MA, Kriebel D, Smith TJ. 1995. Epidemiologic application of a dosimetric model of dust overload. Am J Epidemiol 141:690–696.

Binhi VN. 2002. Magnetobiology: Underlying physical problems. San Diego: Academic Press.

Binhi V. 2008. Do naturally occurring magnetic nanoparticles in the human body mediate increased risk of childhood leukaemia with EMF exposure? Int J Radiat Biol 84:569–579.

Bowman JD. 1998. Calculating exposure metrics from three-axis EMF waveform data. In: Bowman JD, Kelsh MA, Kaune WT, editors. Manual for measuring occupational electric and magnetic field exposures. Cincinnati: National Institute for Occupational Safety and Health. pp III-903-1–III-903-4.

Bowman JD, Thomas DC, London SJ, Peters JM. 1995. Hypothesis: The risk of childhood leukemia is related to combinations of power-frequency and static magnetic fields. Bioelectromagnetics 16:48–59.

Bowman JD, Gailey PC, Gillette LM, Lotz WG, Overton D. 2000. Proceedings of a joint NIOSH/DOE workshop on ''EMF exposure assessment and epidemiology: Hypotheses, metrics, and measurements''. NTIS Report PB 2000-1010 86, National Technical Information Service, Arlington, VA.

Bowman JD, Yue M, Miller CK. 2005. Search for proteins with an ion binding site that has the symmetry necessary for ion parametric resonance. 27th Ann. Mtg. Bioelectromagnetics Soc., Dublin, Ireland, Abstract Collection, pp. 233–237.

Bowman JD, Sahl JD, Krieg EF, Kavet R. 2010. Electric utility worker exposures to biologically based metrics for ELF and static magnetic fields: Job/environment exposure matrices measured by the Multiwave System III. (in preparation).

Burch JB, Reif JS, Yost MG, Keefe TJ, Pitrat CA. 1999. Reduced excretion of a melatonin metabolite in workers exposed to 60 Hz magnetic fields. Am J Epidemiol 150:27–36.

Burstyn I. 2004. Principal component analysis is a powerful instrument in occupational hygiene inquiries. Ann Occup Hyg 48:655–661.

Campbell WC. 1997. Introduction to geomagnetic fields. Cambridge: Cambridge University Press.

Carroll RJ, Ruppert D, Stefanski LA, Crainiceanu CM. 2006. Measurement error in nonlinear models: A modern perspective. Boca Raton, FL: Chapman & Hall/CRC Press.

Engstrom S, Bowman JD. 2004. Magnetic resonances of ions in biological systems. Bioelectromagnetics 25:620–630.

Electric Research and Management (ERM). 1997. Multiwave(R) System II User's Manual: Portable magnetic field measurement concept for transient and steady state fields. Version 4.60T. Pittsburgh, PA: Electric Research and Management, Inc.

Friedman N. 2004. Inferring cellular networks using probabilistic graphical models. Science 303:799–805.

Gandhi OP, Kang G, Wu D, Lazzi G. 2001. Currents induced in anatomic models of the human for uniform and nonuniform power frequency magnetic fields. Bioelectromagnetics 22: 112–121.

Hore PJ. 2005. Rapporteur's report: Sources and interaction mechanisms. Prog Biophys Mol Biol 87:205–212.

International Commission for Non-Ionizing Radiation Protection (ICNIRP). 1998. Guidelines for limiting exposure to time-varying electric, magnetic, and electromagnetic fields (up to 300 GHz). Health Phys 74:494–522.

IEEE International Committee on Electromagnetic Safety. 2002. IEEE Standard for safety levels with respect to human exposure to electromagnetic fields, 0–3 kHz. C95.6. New York, NY: Institute of Electrical and Electronic Engineers.

Kaune WT, Davis S, Stevens RG, Mirick DK, Kheifets L. 2001. Measuring temporal variability in residential magnetic field exposures. Bioelectromagnetics 22:232–245.

Kheifets L, Bowman JD, Checkoway H, Feychting M, Harrington JM, Kavet R, Marsh G, Mezei G, Renew DC, van Winjgaarden E. 2009. Future needs of occupational epidemiology of extremely low frequency (ELF) electric and magnetic fields (EMF): Review and recommendations. Occup Environ Med 66:72–80.

Kriebel D, Smith TJ. 1990. A nonlinear pharmacologic model of the acute effects of ozone on the human lungs. Environ Res 51: 120–146.

Lednev VV. 1995. Comments on ''Clarification and application of ion parametric resonance model for magnetic field interactions with biological systems'' by Blanchard and Blackman. Bioelectromagnetics 16:268–269.

McDevitt JJ, Breysse PN, Bowman JD, Sassone DM. 2002. Comparison of extremely low frequency (ELF) magnetic field personal exposure monitors. J Exp Anal Environ Epidemiol 12:1–8.

Morgan MG, Nair I. 1992. Alternative functional relationships between ELF field exposure and possible health effects: Report on an expert workshop. Bioelectromagnetics 13:335–350.

Polk C. 1994. Effects of extremely-low-frequency magnetic fields on biological magnetite. Bioelectromagnetics 15: 261–270.

Press WH, Flannery BP, Teukolosky SA, Vetterling WT. 1988. Cubic spline interpolation. In: Numerical recipes in C. Cambridge: Cambridge University Press. pp 94–98.

Reinsch CH. 1967. Smoothing by spline functions. Numer Math 10:177–183.

SAS. 2003. The DISCRIM Procedure, SAS OnlineDoc9. Cary, NC: SAS Institute, Inc. (last accessed November 24, 2009). http://support.sas.com/91doc/docMainpage.jsp.

Savitz DA, Ohya T, Loomis DP, Senior RS, Bracken TD, Howard RL. 1994. Correlations among indices of electric and magnetic field exposure in electric utility workers. Bioelectromagnetics 15:193–204.

SOM. 2010a. Motion correction algorithm. Bioelectromagnetics, Supplementary Online Material, Section 1, pp 1–2. http://www3.interscience.wiley.com/journal/34135/home.

SOM. 2010b. Motion test. Bioelectromagnetics, Supplementary Online Material, Section 2, pp 2–3. http://www3.interscience.wiley.com/journal/34135/home.

SOM. 2010c. Cutoffs for digital noise filters. Bioelectromagnetics, Supplementary Online Material, Section 3, p. 4. http://www3.interscience.wiley.com/journal/34135/home.

SOM. 2010d. Correction for the bias in RMS[dB/dt] from spline smoothing. Bioelectromagnetics, Supplementary Online Material, Section 4, p. 5. http://www3.interscience.wiley.com/journal/34135/home.

SOM. 2010e. Model for induced electric fields. Bioelectromagnetics, Supplementary Online Material, Section 5, pp 5–6. http://www3.interscience.wiley.com/journal/34135/home.

SOM. 2010f. Software details. Bioelectromagnetics, Supplementary Online Material, Section 6, pp 7–8. http://www3.interscience.wiley.com/journal/34135/home.

Stayner L, Kuempel E, Gilbert S, Hein M, Dement J. 2008. An epidemiological study of the role of chrysotile asbestos

fibre dimensions in determining respiratory disease risk in exposed workers. Occup Environ Med 65:613–619.

Villeneuve PJ, Agnew DA, Corey PN, Miller AB. 1998. Alternate indices of electric and magnetic field exposures among Ontario electrical utility workers. Bioelectromagnetics 19: 140–151.

World Health Organization (WHO). 2007. Extremely low frequency fields: Environmental health criteria 238. Geneva, Switzerland: WHO.

Woskie SR, Smith TJ, Hallock MF, Hammond SK, Rosenthal F, Eisen EA, Kriebel D, Greaves IA. 1994. Size-selective pulmonary dose indices for metal-working fluid aerosols in machining and grinding operations in the automobile manufacturing industry. Am Ind Hyg Assoc J 55: 20–29.

Zhang J, Nair I, Sahl J. 1997. Effects function analysis of ELF magnetic field exposure in the electric utility work environment. Bioelectromagnetics 18:365–375.